

## Article

# Research on Tunable SPR Sensors Based on WS<sub>2</sub> and Graphene Hybrid Nanosheets

Di Wang <sup>1</sup> , Jin Liu <sup>1,\*</sup>, Haima Yang <sup>2</sup> , Bo Huang <sup>1</sup> and Guohui Zeng <sup>1</sup>

<sup>1</sup> School of Electronic and Electrical Engineering, Shanghai University of Engineering Science, Shanghai 201620, China; m025120321@sues.edu.cn (D.W.); huangbosues@sues.edu.cn (B.H.); zenggh@sues.edu.cn (G.Z.)

<sup>2</sup> School of Optical-Electrical and Computer Engineering, University of Shanghai for Science and Technology, Shanghai 200093, China; snowyhm@sina.com

\* Correspondence: flyingpine@sina.com; Tel.: +86-137-6193-6139

**Abstract:** A prismatic excitation-based affinity biosensor consisting of the prism (BK7), WS<sub>2</sub>/graphene hybrid nanosheets, and silver (Ag) as the active metal for the surface plasmon resonance is proposed in this present research. The introduction of the transition metal WS<sub>2</sub>/graphene layer protected the silver substrate and enhanced the adsorption of biomolecules, which facilitated the quality and performance of detection. Here, we improved the detection structure by focusing on the metallic materials, graphene and WS<sub>2</sub> film layers, and the thickness of the measured medium on the sensing effect. The results show that the silver film had a more desirable resonance effect, and the design of the symmetric detection structure produced a double resonance peak, and it provides a reference for distributed sensing. Changing the thickness of the detection medium can dynamically adjust the wave vector matching conditions, which gives the sensor a certain tunability. In the bilayer WS<sub>2</sub> and monolayer graphene ( $W = 2$ ,  $G = 1$ ) configuration, the sensitivity was up to 224 deg/RIU with a quality factor of 96.97 RIU<sup>-1</sup>, which has potential for clinical analytic and biochemical detecting applications.



**Citation:** Wang, D.; Liu, J.; Yang, H.; Huang, B.; Zeng, G. Research on Tunable SPR Sensors Based on WS<sub>2</sub> and Graphene Hybrid Nanosheets. *Photonics* **2022**, *9*, 490. <https://doi.org/10.3390/photonics9070490>

Received: 13 June 2022

Accepted: 8 July 2022

Published: 12 July 2022

**Publisher's Note:** MDPI stays neutral with regard to jurisdictional claims in published maps and institutional affiliations.



**Copyright:** © 2022 by the authors. Licensee MDPI, Basel, Switzerland. This article is an open access article distributed under the terms and conditions of the Creative Commons Attribution (CC BY) license (<https://creativecommons.org/licenses/by/4.0/>).

## 1. Introduction

Since the first commercial SPR sensor was introduced in 1990, surface plasmon resonance technology, derived from physical optical phenomena, has gained widespread attention [1]. Free electrons at the interface of metals and dielectrics are excited by p-polarized light at a specific angle to form a collective vibration of the surface plasmon excitation wave (SPW). Part of the polarized light penetrates the metal and becomes an evanescent wave with exponential attenuation. When two wave vectors are coordinated, the immediate result is a sharp decrease in the energy of the detected reflected light, because the energy in the photons has been transferred in the process [2]. SPR-based biosensors are currently the focus of numerous studies due to the fact of their nondestructive inspection without specific markers for high-accuracy work requirements online, showing great potential in drug screening [3,4], environmental monitoring [5,6], biochemistry [7], and other fields.

A Kretschmann structure is often applied in SPR sensors, and gold (Au) and silver (Ag) materials usually act as the application film layers [8]. The gold film is chemically stable and has good corrosion and oxidation resistance; the disadvantage is that it has poor biomolecular binding capacity. Silver and aluminum films can produce sharper resonance peaks with higher sensitivity [9], but the shortcoming is that they are easily oxidized. In addition, copper resonance peaks are relatively too wide. To improve the detection quality of sensing devices, it is a common practice to make improvements in structure and materials [10]. Thanks to the rapid development of nanotechnology, some scholars

have introduced metal nanoparticles into the plasma material film coupled to the sensor to produce localized surface plasmon resonance to improve detection accuracy [11]. For example, Morisawa, H. et al. prepared a hole array model using an aluminum disc and found that the electric field in the hole and cavity of the aluminum disc would be strongly coupled, resulting in a 400% increase in photon emission efficiency [12]. At the same time, the use of fiber optic piggyback plasma materials for sensing and detection to achieve remote real-time online detection has achieved certain achievements [13–15]. However, these approaches are extremely demanding in terms of the preparation process and pose difficult challenges in terms of cost and the realization of mass produced applications. The introduction of novel plasma materials into metallic material structures is now considered among the most successful techniques for improving SPR sensor performance, which can be used to prepare sensing chips on a large scale.

Two-dimensional nanomaterials are widely used because of their mechanical flexibility for complex structural designs and their efficient carrier mobility and optical transparency that allow them to have good optoelectronic properties [16]. Karki, B. [17] et al. introduced black phosphorus and newly developed brassies (e.g., BaTiO<sub>3</sub>) into SPR sensors based on the excellent performance of two-dimensional nanomaterials; it showed that the sensitivity improved by 0.55, 1.5, and 1.86 times, respectively, relative to the conventional gold-, silver-, copper-based sensors. The detection accuracy of the biosensor was enhanced by using zinc oxide and blue phosphorus molybdenum disulfide heterostructures. The proposed SPR sensor can be practically applied in SPR chips and can detect biomolecules in the visible light range [18]. In medical detection of hemoglobin and blood glucose levels, Mostufa, S. [19] et al. introduced graphene coating to SPR sensors and increased the maximum sensitivity to 200 deg/RIU. Ouyang et al. designed structures with different combinations of 2D nanomaterials and silicon nanosheets to explore the effect of enhanced sensing performance, and the structures exhibited good sensing performance. Finally, they compared the functional differences among MoS<sub>2</sub>/MoSe<sub>2</sub>/WS<sub>2</sub>/WSe<sub>2</sub> [20]. They are not just surrounding materials with a contrasting refractive index for silver. With a surface area of 2630 m<sup>2</sup>/g and a rich π-conjugated structure, graphene is suitable for the direct interaction of biomolecules and provides good support for biomolecule adsorption, which is suitable for the dielectric top layer of SPR sensing. The transition metal, WS<sub>2</sub>, is chemically stable in addition to its induced strong coupling properties [21]. Covering the surface of the metal layer protects the silver substrate and enhances the adsorption of biomolecules with the graphene on the surface, which plays an important role in the study of biomolecular interactions and contributes to the quality and performance of the assay. WS<sub>2</sub> nanosheet overlays are also able to show additional benefits such as tunability in the resonant wavelength region, biocompatibility, vapor capacity, and gas sensitivity.

This study designed a symmetrical sensing device formed by stacking graphene and WS<sub>2</sub> hybrid nanostructures on a silver substrate. The choice of silver film sharpened the reflection curve, and the unique optoelectronic properties of graphene and WS<sub>2</sub> contributed to the improvement of the sensor's sensitivity and quality factors. Analysis of the sensing characteristics of this SPR symmetric structure was performed using angular modulation and optimization of the factors affecting the performance of the type. The absorption characteristics of the graphene and WS<sub>2</sub> materials were carried out using the optical simulation FDTD method, and the number of layers was optimized to further develop the detection structure's sensitivity. Changing the thickness of the detection medium can dynamically adjust the incident light angle range, which gives the sensor a certain degree of tunability.

## 2. Theory and Mathematical Analysis

### 2.1. Design Consideration

The proposed symmetrical tunable SPR biosensor with a Ag-WS<sub>2</sub>-Graphene heterostructure consists of eight layers, and Figure 1 shows its structure. Firstly, prism (BK7) was selected as the substrate, and silver was deposited on the prism substrate. The wave-

length was set to 632.8 nm, causing the optical nonlinearity to be enhanced at this frequency. Then WS<sub>2</sub> and graphene nanofilms were sequentially precipitated on the silver layer to achieve an interlayer structure between the silver and affinity layers (where W and G represent the number of WS<sub>2</sub> and graphene film layers). The coupling model was mounted on a high-precision rotating device to facilitate scanning of incident light at different angles, and then the beam from the He-Ne laser was incidental on the coupling prism after passing through the polarizer to excite the SPR effect. The middle region of the symmetric prism in the model formed the flow cell of the detection medium. When the refractive index of the liquid in the flow cell changed, the resonance angle shifted, and the signal was transmitted to the detector in real time and analyzed to obtain the concentration of analytes and other parameter changes. Table 1 shows the detailed specifications and parameters.

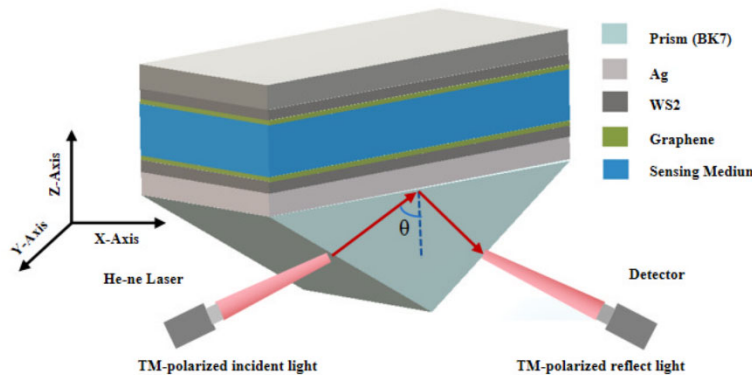


**Figure 1.** Proposed model of symmetrical surface plasmons resonance sensor.

**Table 1.** Geometrical and physical parameters of the SPR sensor at 632.8 nm.

Material	Refractive Index (Real Part)	Refractive Index (Imaginary Part)	The Thickness of the Layer (nm)
BK7	1.5151	$1.2122 \times 10^{-8} \times i$	—
Ag	0.056253	$4.2760 \times i$	40
WS <sub>2</sub>	5.0777	$0.43515 \times i$	$W \times 0.8$
Graphene	2.4105	—	$G \times 0.34$
Sensing medium	1.330–1.370		200–500

## 2.2. Mathematical Modeling for Reflectivity

In this typical Kretschmann configuration, SF10, sulfur prisms, or silicon carbide are usually chosen as coupling prisms, and in this paper, the BK7 prism with a lower refractive index was chosen to facilitate the sensing performance. The refractive index (RI) of the BK7 glass, as a function of the wavelength of P-polarized light, was calculated by the following relations:

$$n_{BK7} = \left( \frac{1.03961212\lambda^2}{\lambda^2 - 0.00600069867} + \frac{0.231792344\lambda^2}{\lambda^2 - 0.0200179144} + \frac{1.03961212\lambda^2}{\lambda^2 - 103.560653} \right)^{1/2} \quad (1)$$

where  $\lambda$  is the wavelength of the optical signal. A silver film 40 nm thick was chosen as the SPR active material, which had a refractive index that can be expressed as follows according to the Drude model:

$$n_{metal} = \sqrt{\epsilon_m} = \left( 1 - \frac{\lambda_c \lambda^2}{\lambda_p^2 (\lambda_c + i\lambda)} \right)^{1/2} \quad (2)$$

where the  $\lambda$  value is set to 632.8 nm;  $\lambda_p$  and  $\lambda_c$  of silver (Ag) is taken as  $1.4541 \times 10^{-7}$  m and  $1.7641 \times 10^{-5}$  m. The RI of WS<sub>2</sub> can be calculated as  $5.0777 + 0.43515 * i$ , with the thickness is  $D \times 0.8$  nm ( $W$  represents the number of WS<sub>2</sub> layers). The refractive index of graphene can be shown below [22]:

$$n_G = 3 + \frac{iC_1}{3}\lambda \quad (3)$$

where  $C_1 = 5.446 \mu\text{m}^{-1}$  and  $\lambda$  represent the optical signal wavelength. In the experiment,  $G$  denotes the number of graphene layers, and the thickness is expressed as  $T_G = G \times 0.34$  nm. Silver layers can be deposited by electron beam evaporation or sputtering techniques and graphene/WS<sub>2</sub> by chemical vapor deposition (CVD) techniques. The grown samples were first observed by optical microscopy, and the monolayer of WS<sub>2</sub> could be initially distinguished by the difference in color on the substrate. Then, the distinguished samples were subjected to Raman and PL spectroscopy to further confirm the analysis. AFM was next used to determine the prepared WS<sub>2</sub> as a monolayer, and the crystalline quality of the monolayer WS<sub>2</sub> prepared using the CVD method could be further investigated by XSP as well as STEM tests. Finally, the prepared monolayer of WS<sub>2</sub> was transferred to the Ag substrate using the wet transfer method. The material layers in the structure were arranged in the  $z$ -axis direction, where  $V$  and  $U$  denote the magnetic field component and electric field component at the limit constraint surface. The tangential components of the first and last layers can be linked with the following equation [23]:

$$\left[ \frac{U_1}{V_1} \right] = M \left[ \frac{U_{N-1}}{V_{N-1}} \right] \quad (4)$$

where  $M$  stands for the characteristic matrix of the sensor combination structure, which is derived from the sequential layer matrix. It can be written as:

$$M = \prod_{k=2}^{N-1} M_i = \begin{bmatrix} M_{11} & M_{12} \\ M_{21} & M_{22} \end{bmatrix} \quad (5)$$

with

$$M_i = \begin{bmatrix} \cos \beta_i & -i \sin \beta_i / \chi_i \\ -i \chi_i \sin \beta_i & \cos \beta_i \end{bmatrix} \quad (6)$$

In the above equation,  $\beta_i = \frac{2\pi d_i (\epsilon_i - n_1^2 \sin^2)^{1/2}}{\lambda}$ ,  $\beta_i = \frac{(\epsilon_i - n_1^2 \sin^2)^{1/2}}{\epsilon_i}$ , and  $\chi_i = \frac{(\epsilon_i - n_1^2 \sin^2)^{1/2}}{\epsilon_i}$ . The principle of the transmission matrix of the  $n$ -layer film can be applied to analyze the TM polarization mode, from which we can obtain four elements:  $M_{11}$ ,  $M_{12}$ ,  $M_{21}$ , and  $M_{22}$ . Bringing them into the reflection coefficient calculation formula, one can obtain the following relationship:

$$r_p = \frac{(M_{11} + M_{12}\chi_N)\chi_1 - (M_{21} + M_{22}\chi_N)}{(M_{11} + M_{12}\chi_N)\chi_1 + (M_{21} + M_{22}\chi_N)} \quad (7)$$

Combining the above analysis, the reflectivity of p-polarized light can be expressed by the following analytical formula [24]:

$$R = |r_p|^2 \quad (8)$$

### 2.3. Mathematical Modeling for Reflectivity

High sensitivity is one of the primary marks of a decent sensor execution, which mirrors the capacity of the sensor to answer small changes in the refractive file of the recognized substance. The increase in the refractive index of the detection medium will cause a shift in the reflectivity curve at the same time; meanwhile, the corresponding

attenuation angle will change. Therefore, the sensitivity can be defined as the ratio of the corresponding angular shift of the decaying peak to the amount of change in the refractive index of the medium, expressed in an analytical formula as:

$$S = \frac{\Delta\theta_{SPR}}{\Delta n_a} \quad (9)$$

The detection accuracy (*D.A.*) of SPR sensors is strongly influenced by the reflectivity curve's full width at the half maximum (*FWHM*), which is defined as:

$$D.A = \frac{\Delta\theta_{SPR}}{FWHM} \quad (10)$$

Finally, the quality factor (*Q.A.*) of the sensor is also an important performance parameter, which is influenced by the sensitivity and the full width at the half maximum of the reflectivity curve; therefore, it can be determined by the following formula:

$$Q.F = S/FWHM(RIU)^{-1} \quad (11)$$

### 3. Results and Discussion

#### 3.1. Impact of Metal Selection Optimization on Sensor Performance

In angle modulation-based SPR sensors, the choice of the metal layer material has a significant influence on the sensitivity. This device mainly analyzes the widely used gold (Au) and silver (Ag) materials and studies their resonance characteristics through simulation and comparison. A 632.8 nm monochromatic light source was used, and the incident prism was a BK7 glass that had a refractive index of 1.515. Structure 1 was a conventional gold substrate SPR sensor with gold as the metal film. The thickness was set to 40 nm, and the medium was pure water with a refractive index of 1.330. Structure 2 was the symmetrical BK7 prism/silver detection media structure. The thickness of the silver film was 40 nm, and the detection media thickness was 400 nm. Keeping the other experimental conditions, the relationship between normalized light intensity and angle, the reflectance spectra, and the electrical field distribution of different structures of metal film layers resonating with water was obtained as shown in Figure 2.

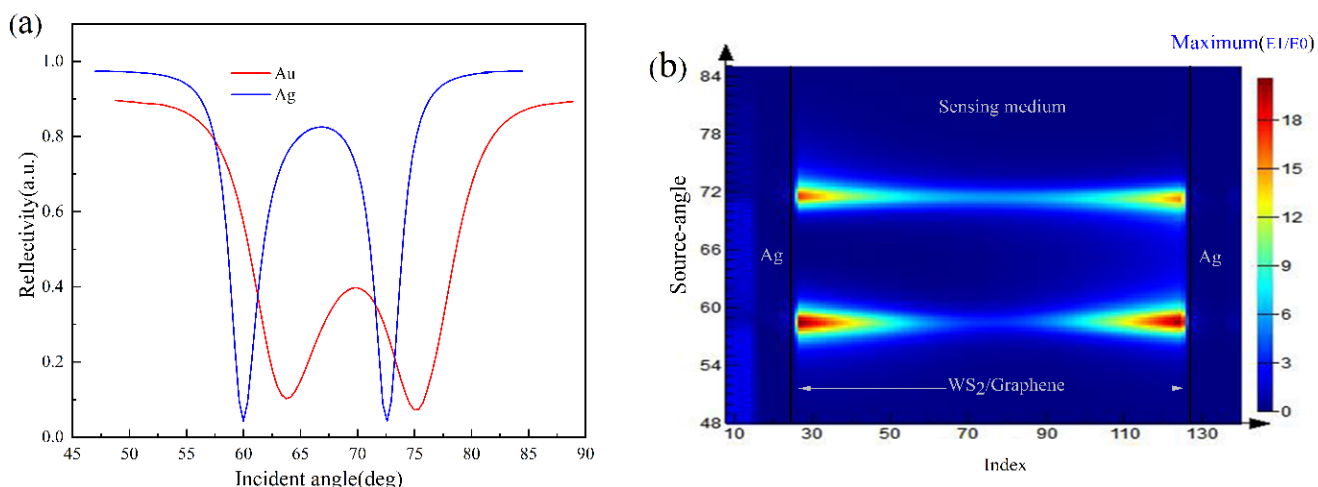


**Figure 2.** Comparison of reflectance curves and electric field diagrams for symmetrical gold and symmetrical silver films: (a) resonance response curves of different metal materials; (b) SPR corresponding to the electrical field intensity distribution diagrams at a symmetrical structure silver film thickness of 40 nm and detection medium thickness of 400 nm.

As it can be seen in Figure 2a, contrasted with customary gold film SPR sensors, the symmetrical silver film structure had sharper attenuation peaks and smaller half-height widths in the reflectivity curve, which implies the sensor's recognition exactness and quality factor were obtained at a higher level. Figure 2b,c shows the optical distribution of two model resonances, and it can be seen that most of the light in the symmetric structure was confined in the detection medium layer, with little light in the surrounding environment relative to the conventional SPR sensing device with a gold substrate, which contributes to the sensitivity and environmental independence of the system.

After the advantages of the silver layer were determined, we further optimized the depth of the silver (Ag). Structures with different thicknesses of silver layers (i.e., 35, 40, 45, and 50 nm) were selected for analysis and comparison, and their reflectivity curves are displayed in Figure 3. Meanwhile, Figure 3b plots the trends of the resonance peaks' full width at the maximum (FWHM) and minimum resonance response when the thickness of the silver film was varied. From the two figures, it can be found that the attenuation peak depth was deeper when the silver layer thickness was set to 40 nm, and the two attenuation peaks did not overlap. At this time, the sharper resonance curve was beneficial to the improvement of the quality factor.

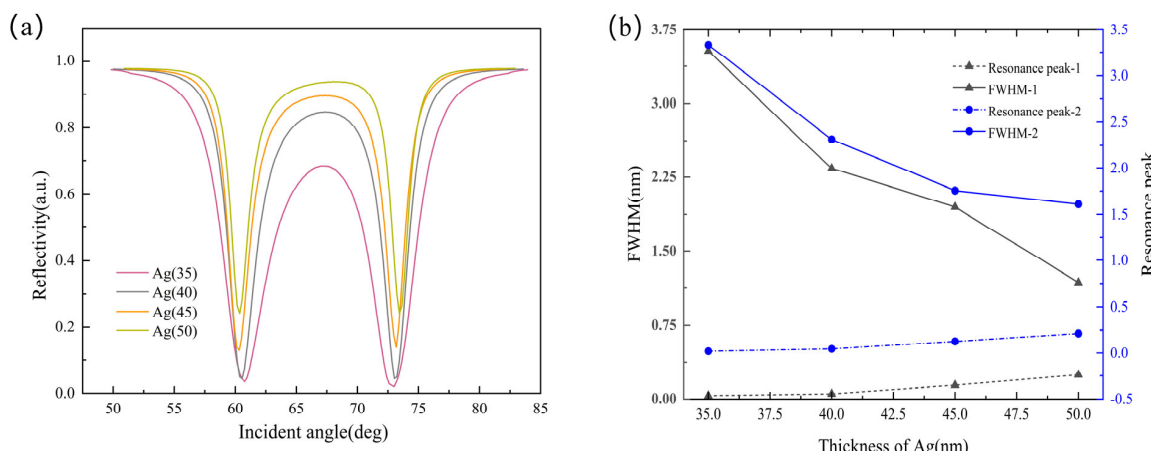


**Figure 3.** (a) Reflectance versus angle curve for different metal thicknesses; (b) variations in the half-height width and reflectivity minimum with the thickness of the silver (Ag) layer.

### 3.2. Effect of Membrane Layer Structure on SPR Sensing Performance

Considering that silver nanofilms are easily oxidized and have poor stability in the air, which affects the sustainability and reproducibility of sensor performance. It was found that improvements could be made by introducing 2D materials. In this section, to investigate the extent to which  $\text{WS}_2$  and graphene affect the sensor performance, four symmetric structures (i.e., monolayer silver, silver/graphene, silver/ $\text{WS}_2$ , and silver/graphene/ $\text{WS}_2$ ) were introduced to evaluate the improvements made in the proposed model. Figure 4 plots the reflectance function curves as well as the sensitivity values for the different structures under the same medium refractive index variation, and the performance parameters of the four structures are shown in Tables 2 and 3.

**Table 2.** The performance of the above four structures at a medium refractive index change gradient of 0.005 (the first decaying peak).

S.N	Structure (Membrane Layer on One Side)	Sensitivity (deg/RIU)	FWHM (°)	DA ( $\text{Degree}^{-1}$ )	FOM ( $\text{RIU}^{-1}$ )
a	BK7-silver(Ag)-detection medium	130.76	2.24	0.292	58.38
b	BK7-silver(Ag)-graphene-detection medium	148.64	2.39	0.311	62.19
c	BK7-silver(Ag)- $\text{WS}_2$ -detection medium	170.18	2.46	0.346	69.18
d	BK7-silver(Ag)- $\text{WS}_2$ -graphene-detection medium	186.06	2.49	0.373	74.72

**Table 3.** The performance of the above four structures at a medium refractive index change gradient of 0.005 (the second decaying peak).

S.N	Structure (Membrane Layer on One Side)	Sensitivity (deg/RIU)	FWHM (°)	DA (Degree <sup>-1</sup> )	FOM (RIU <sup>-1</sup> )
a	BK7-Silver(Ag)-Detection medium	138.82	2.16	0.321	64.27
b	BK7-Silver(Ag)-Graphene-Detection medium	152.82	2.24	0.341	68.22
c	BK7-Silver(Ag)-WS <sub>2</sub> -Detection medium	172.16	2.31	0.372	74.53
d	BK7-Silver(Ag)-WS <sub>2</sub> -Graphene-Detection medium	213.04	2.41	0.441	88.40

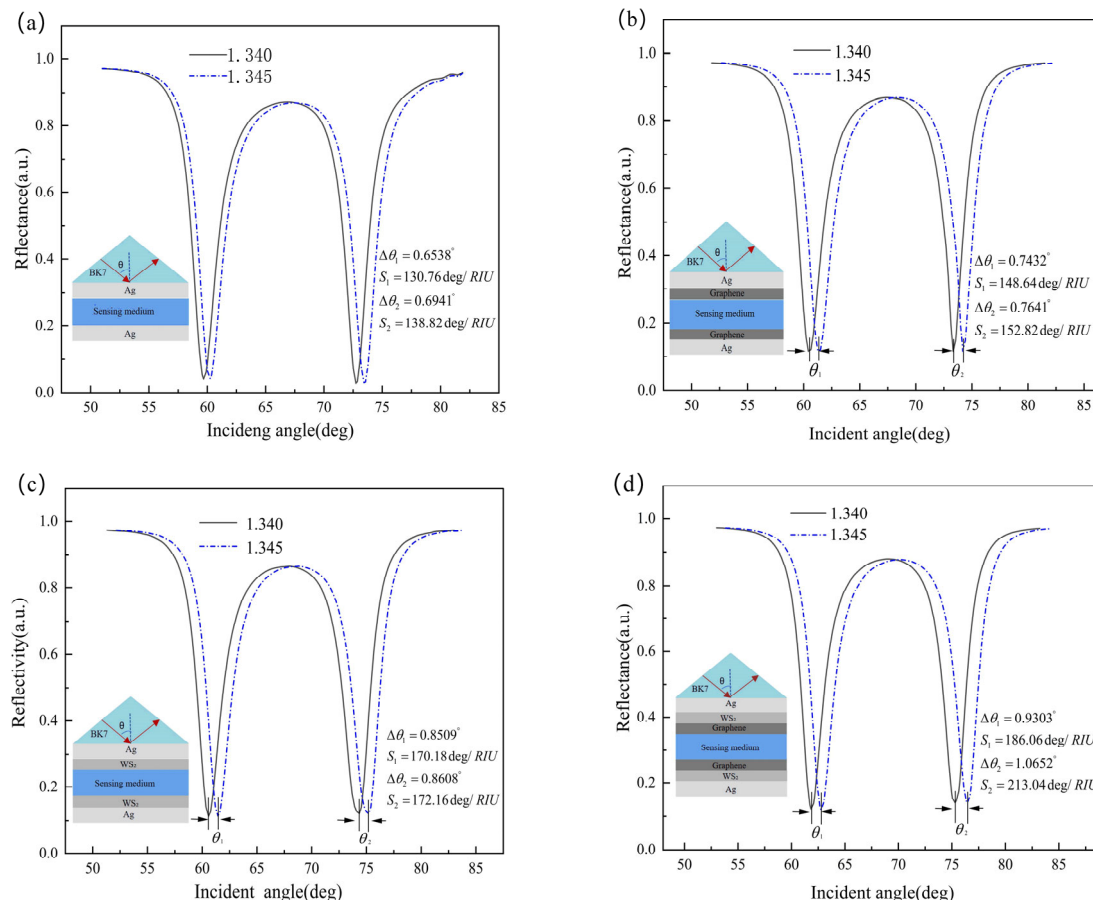


**Figure 4.** The reflectance and incident angle varied with ws<sub>2</sub> and graphene for the same gradient change in RI: (a) only the 40 nm silver layer configured ( $W = 0, G = 0$ ); (b) configured with the 40 nm silver and the monolayer of graphene ( $W = 0, G = 1$ ); (c) configured with the 40 nm silver and the monolayer of WS<sub>2</sub> ( $W = 1, G = 0$ ); (d) simultaneous configuration of 40 nm silver, the monolayer of WS<sub>2</sub> and graphene ( $W = 1, G = 1$ ).

By comparing the above data, it can be found that WS<sub>2</sub> and graphene can make strides in the performance of the sensor to a certain degree compared with the traditional silver-based SPR sensor. When WS<sub>2</sub> and graphene ( $W = 1, G = 1$ ) were stacked, the maximum resonance angle shift increased from  $0.6941^\circ$  to  $1.0652^\circ$ , and the sensing performance improved by 53.5% with a sensitivity of  $213.04 \text{ deg/RIU}$ . Meanwhile, the maximum values of detection accuracy and quality factor were  $0.441$  and  $88.40 \text{ RIU}^{-1}$ , respectively, both of which showed significant improvements.

### 3.3. WS<sub>2</sub> and Graphene Layer Optimization

In the above study, it was found that the introduction of WS<sub>2</sub> and graphene was confirmed to advance the performance of the sensor, and the sensor would have different

performance parameters when the thickness of  $\text{WS}_2$  and graphene changed. Therefore, this section focuses on the optimization of  $\text{WS}_2$  and graphene layering.

Figure 5 shows the resonance curves of  $\text{WS}_2$  and graphene from 1 layer gradually increasing to 5 layers. It can be seen that the detected reflectance became progressively larger with the increasing thickness of both materials; those factors all cause the attenuation peak to migrate to a larger angle corresponding to the reflection angle, the reflectance curve to become wider, and the value of the width at the maximum to become progressively larger, which implies a decrease in detection accuracy. In addition, this effect was more obvious when tungsten disulfide was added. Therefore, the solution to breakthrough sensing performance cannot be sought by blindly adding the thickness of  $\text{WS}_2$  and graphene.

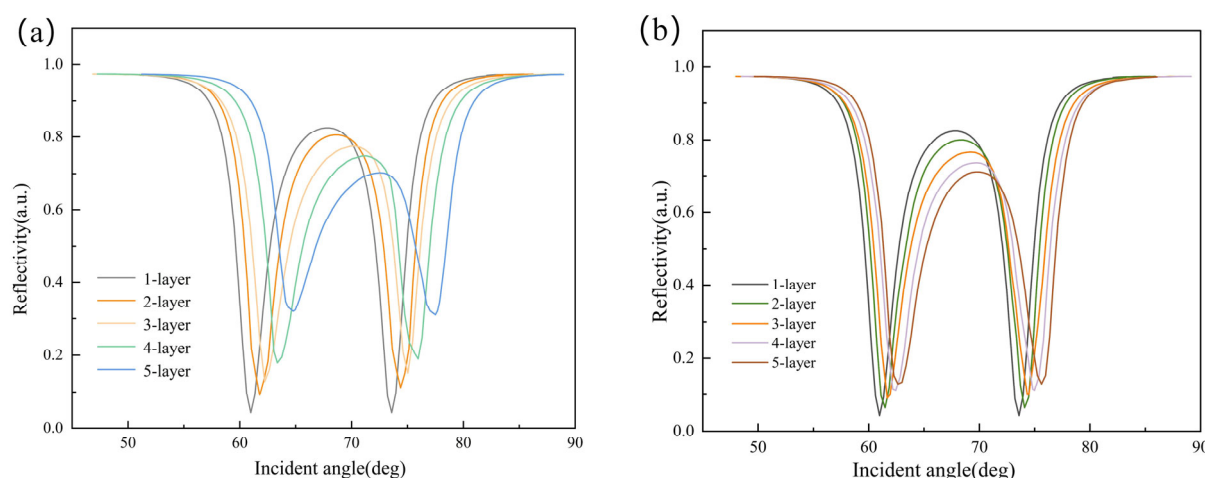


**Figure 5.** Functional relationship between the reflectivity and incident angle: (a) reflectivity curve when graphene was set as a single layer and the  $\text{ws}_2$  layer was added; (b) reflectance function curve when the number of graphene layers was gradually increased ( $\text{WS}_2$  was set to a single layer).

Firstly, the trends in the sensor's sensitivity when stacking different thicknesses of  $\text{WS}_2$  and the sensitivity distribution of the sensors with different  $\text{WS}_2$  structural layers during the gradual increase in the RI of the detection medium (1.330–1.370) were investigated, and they are expressed in Figure 6. It can be analyzed that when the silver layer's thickness was 40 nm and the medium's thickness was 400 nm, the sensitivity did not show a linear increasing trend with the number of  $\text{WS}_2$  layers, and the graphene was set to a single layer at the same time. When the number of layers of  $\text{WS}_2$  exceeded two, the sensor sensitivity started to gradually decrease, which was caused by the decrease in light utilization; thus, the optimized  $\text{WS}_2$  should be set to two layers. It was found that the reflectivity curve showed a maximum offset angle of  $1.12^\circ$  for the second decay peak over the range of refractive index variation of the medium as shown in Figure 6. At this point, the maximum sensitivity reached 224 deg/RIU.

When investigating the relationship between the variations in graphene thickness and sensitivity, we refer to the analysis of  $\text{WS}_2$  (where the silver layer's thickness was set to 40 nm, and the thickness of the detection medium was 400 nm, with the number of  $\text{WS}_2$  layers and the graphene set to a single layer). The results are shown in Figure 7a,b. It can be summarized that the sensitivity of the structure showed a monotonically decreasing trend by gradually stacking graphene relative to the results of  $\text{WS}_2$ . The presence of strong light-matter interactions between the two-dimensional material and the silver film provided good charge transfer and has been shown in many studies to improve the sensitivity of the sensor. The light absorbance of the monolayer graphene was 2.3% in the broad spectral range, and the light absorbance of  $\text{WS}_2$  was higher. The variation in the sensitivity with the number of  $\text{WS}_2$  and graphene layers is depicted in Figures 6 and 7, respectively, and it can be found that both had an optimal number of layers. As the number of layers increased, the resonance angle shifted in the direction of a greater angle, and the reflectivity curve

became shallower, while the full width at half maximum (FWHM) increased. This was because  $\text{WS}_2$ /graphene is a lossy dielectric material with a complex dielectric constant. With the superposition of the two layers, the damping associated with SPS waves in the region of the composite layer increased, leading to a decrease in light utilization and, thus, an increase in the FWHM value, which limits the further improvement of the sensor's sensitivity. Therefore, according to the analysis above, the number of layers of  $\text{WS}_2$  and graphene should be set to one and two layers ( $W = 2, G = 1$ ) to achieve the best sensing effect.

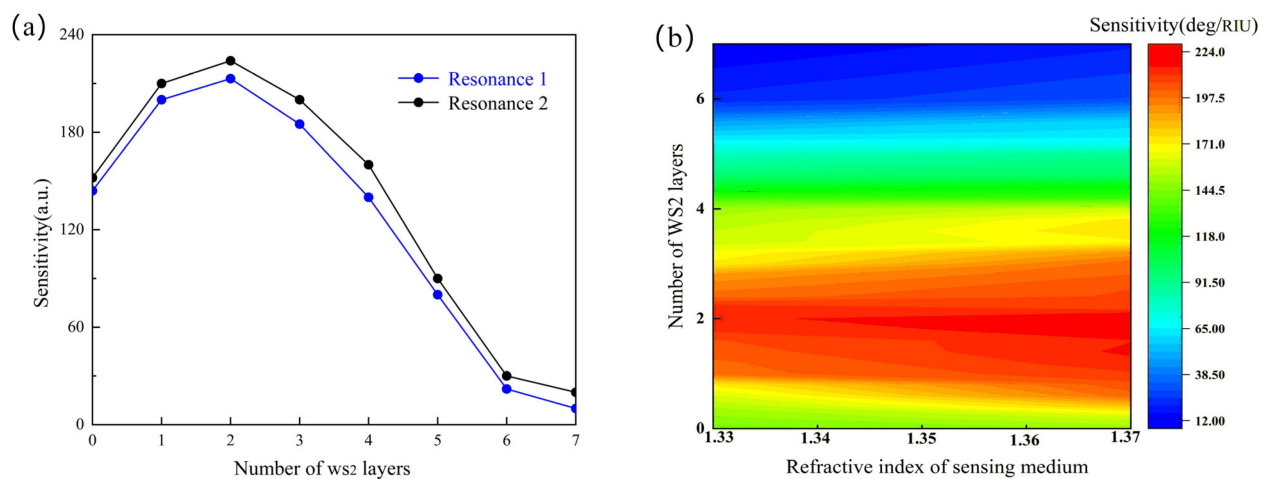


**Figure 6.** (a) Trends in sensor sensitivity when stacking the different thicknesses of  $\text{WS}_2$ ; (b) sensitivity distribution of the sensors with different  $\text{WS}_2$  structural layers during the gradual increase in the RI of the detection medium (1.330–1.370).

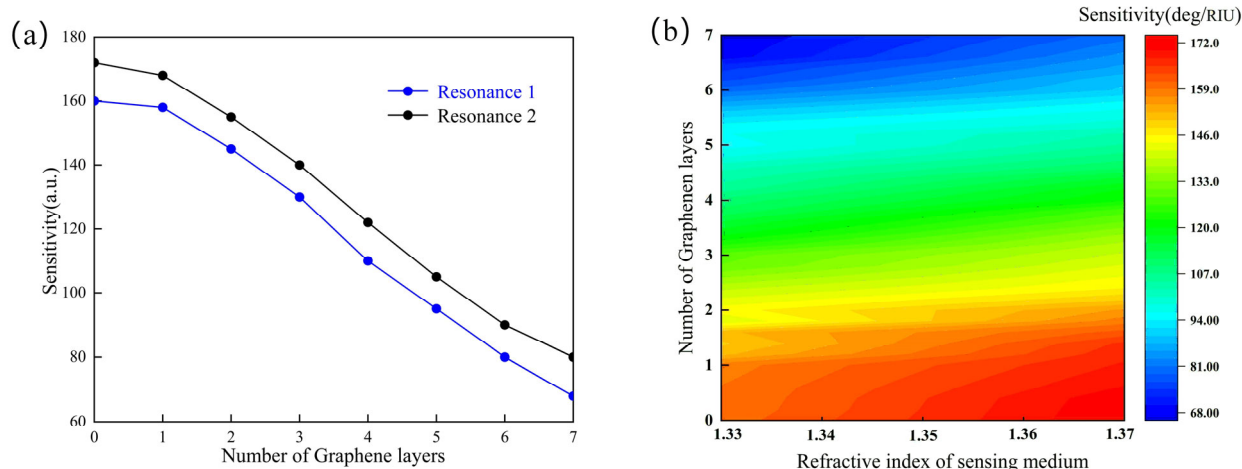


**Figure 7.** (a) Trends in the sensor's sensitivity when stacking different thicknesses of  $\text{WS}_2$ ; (b) sensitivity distribution of the sensors with different  $\text{WS}_2$  structural layers with a gradual increase in the RI of the detection medium (1.330–1.370).

### 3.4. Detect Media Thickness Optimization

The thickness of the detection medium needs to be set within a suitable interval for the detection device to collect the reflectivity curve with a better resonance effect. Therefore, we analyzed the SPR resonance curves of the detection media at 200–500 nm thickness and the corresponding minimum attenuation and half-height width variations as shown in Figure 8.

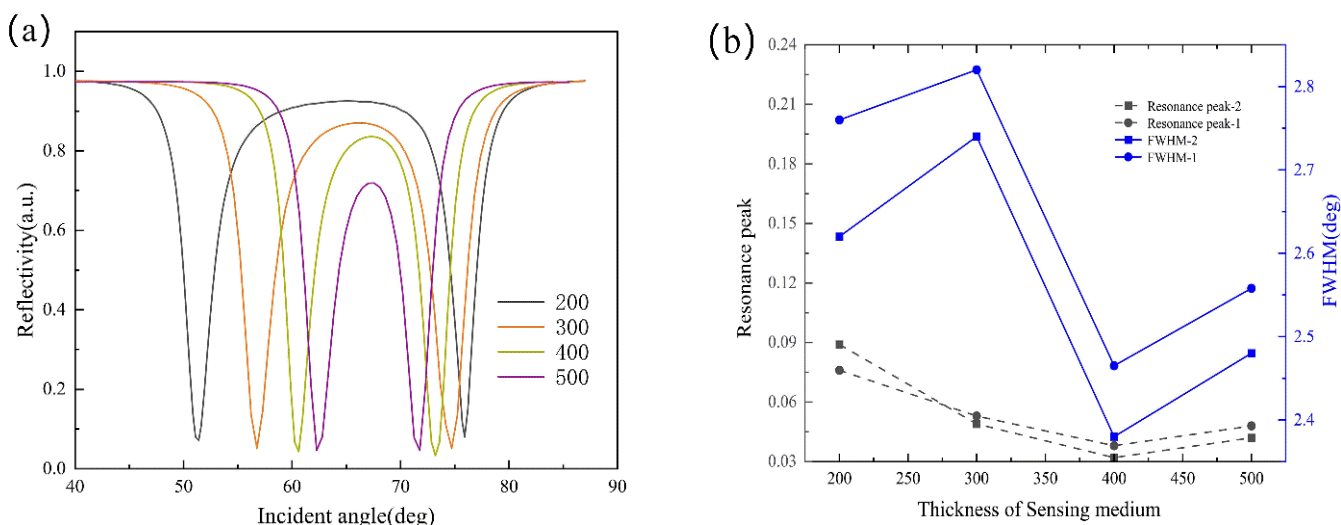


**Figure 8.** (a) Reflectivity variation curve under angle modulation at different detection media thicknesses; (b) half-width height and minimum reflection relationships at different media thicknesses.

It can be seen that in the range of a medium thickness that satisfied the resonance, different medium thicknesses affected the crossover characteristics of the bimodal peaks. When the thickness of the medium was 200–500 nm, the half-height width of the reflectivity curve and the minimum reflection were relatively small for different thicknesses. Therefore, we could selectively adjust the thickness of the medium within a certain range according to the experimental conditions. The thickness of the detection medium could be reduced to 200 nm according to the actual demand, which reduced the sample consumption and also achieved the tunability of the incidence angle range of the sensor.

### 3.5. Performance Analysis and Model Comparison

To further evaluate the practical performance of the designed sensor, experiments were conducted using media with different refractive indices. When the sensing structure was set-up as a symmetric structure with two layers of WS<sub>2</sub>, one layer of graphene, a 40 nm thick silver layer, and a 400 nm thick detection medium, the samples with RI values between 1.330 and 1.370 of the biological samples were detected, and the reflection curves were recorded in real time, and the results are shown in Figure 9a. It can be seen that we obtained good accuracy, half-width height, and resonance peaks in this refractive index range. The relationship between refractive index and the angle of the medium after linear fitting is shown in Figure 9b. The red curve shows the linear fit of the angular mobility of the first decay peak to the change in RI of the detection medium, while the blue curve shows the linear fit of the angular mobility of the second decay peak to the change in RI of the detection medium. From this figure, it can be seen that both attenuation peaks had a good linear relationship (the goodness of fit was greater than 0.99) clearly; thus, the sensor could obtain a good sensing effect by using angle modulation to detect the above refractive index range. It also indicates that the sensor had good sensing performance.

Finally, Table 4 shows a comparison of the sensing performance of the sensing devices based on different models in recent years. It can be found that the structure proposed in this research had a more excellent performance.

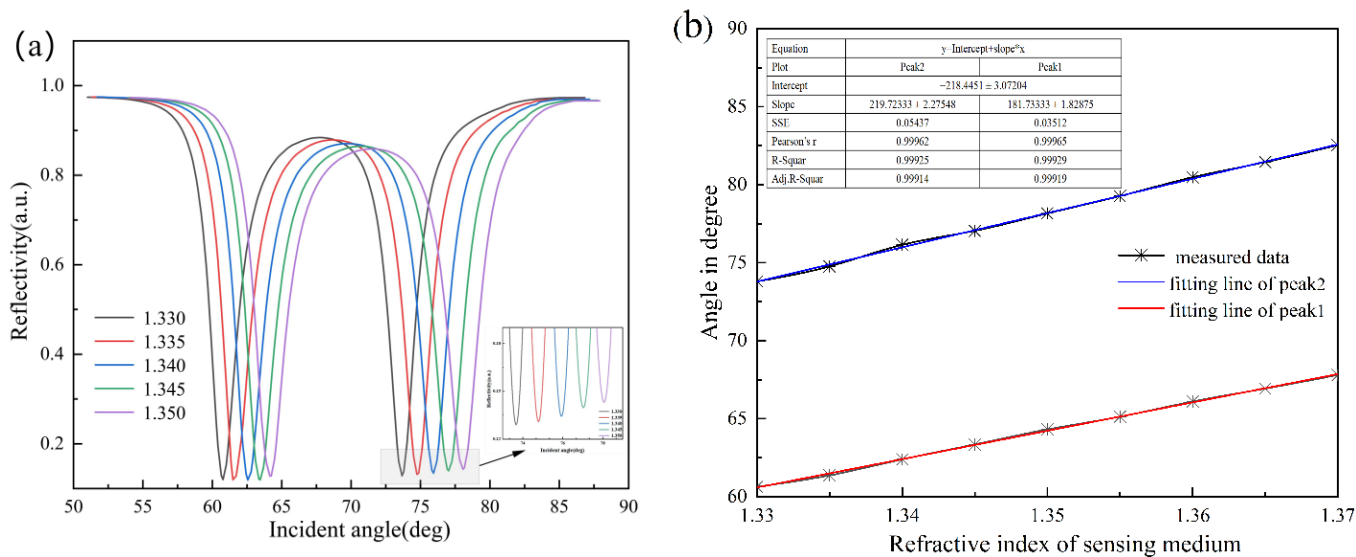


**Figure 9.** (a) Reflectance variation curve with a concentration of detection medium under angle modulation; (b) linear fit of the refractive index versus angle.

**Table 4.** Comparison of the structure and performance of the sensors designed in different studies.

SPR Sensor Structure	Wavelength (nm)	Sensitivity (deg/RIU <sup>-1</sup> )	FWHM (°)	QF (RIU <sup>-1</sup> )	Reference
Bk7 Prism/Ti/Ag/MoS <sub>2</sub> /graphene/BSA	633	144.72	2.24	62.38	[25]
SF10 Prism/Au/ZnO/graphene/sensing medium	633	141.9	9.14	15.53	[26]
SF-10 Glass/Au/BP/graphene/PBS solution	633	125	9.17	13.62	[27]
SF-11 Prism/Au/Ag/TiO <sub>2</sub> /graphene/sensing medium	633	50–180	5.45	18.35	[28]
BK7 Prism/Au/BlueP/MoS <sub>2</sub> heterostructure/graphene/sensing medium	633	204	11.10	18.37	[29]
BK7 Prism/Ag/Au/PtSe <sub>2</sub> /sensing medium	633	165	11.68	14.12	[30]
BK7 Glass/Ag/franckeite/graphene/sensing medium	633	196	4.86	40.29	[31]
Symmetrical BK7 Prism/Ag/WS <sub>2</sub> /sensing medium	632.8	224	2.31	96.97	This Work

#### 4. Conclusions

This research presented a novel SPR sensor. It is a symmetric sensing device formed by stacking WS<sub>2</sub> and graphene hybrid nanostructures on a silver substrate. It demonstrated that the addition of WS<sub>2</sub> and graphene, as the protective layer of the silver base, improved the performance characteristics of the SPR biosensor. We optimized the sensing structure by studying the effects of metallic materials, WS<sub>2</sub> and graphene film layers, and the thickness of the medium under test on the sensing effect. The detection medium had a good resonance curve and sensing characteristics in the range of 1.33 to 1.37 refractive index as a sensing structure when a single graphene layer, a double layer of WS<sub>2</sub>, a 40 nm thick silver layer, and a 400 nm detection medium were used. For the best resonance results and sensing characteristics, the sensitivity was as high as 224 deg/RIU, and the quality factor was 96.97 RIU<sup>-1</sup>. Based on these optimal performance parameters, the proposed symmetrically structured surface plasmon resonance sensor with silver-WS<sub>2</sub>-graphene hybrid nanocoating can be effectively applied in the direction of medical diagnostics and biochemical sensing aspects due to the fact of its good sensing performance.

**Author Contributions:** Conceptualization, D.W.; Data curation, H.Y.; Investigation, D.W. and B.H.; Methodology, J.L.; Project administration, J.L.; Supervision, G.Z. All authors have read and agreed to the published version of the manuscript.

**Funding:** This research was funded by the Shanghai Science and Technology Innovation Action Plan (22S31903700, 21S31904200).

**Institutional Review Board Statement:** Not applicable.

**Informed Consent Statement:** Not applicable.

**Data Availability Statement:** Not applicable.

**Conflicts of Interest:** The authors declare no conflict of interest.

## References

- Cao, E.; Lin, W.; Sun, M.; Liang, W.; Song, Y. Exciton-plasmon coupling interactions: From principle to applications. *Nanophotonics* **2018**, *7*, 145–167. [[CrossRef](#)]
- Lan, G.; Liu, S.; Ma, Y.; Zhang, X.; Wang, Y.; Song, Y. Sensitivity and figure-of-merit enhancements of liquid-prism SPR sensor in the angular interrogation. *Opt. Commun.* **2010**, *87*, 1315–1318. [[CrossRef](#)]
- Wang, D.; Loo, J.F.C.; Lin, W.; Geng, Q.; Ngan, E.K.S.; Kong, S.K.; Yam, Y.; Chen, S.C.; Ho, H.P. Development of a sensitive DMD-based 2D SPR sensor array using single-point detection strategy for multiple aptamer screening. *Sens. Actuators B Chem.* **2020**, *305*, 127240. [[CrossRef](#)]
- Chiu, N.; Tai, M.J.; Nurrohman, D.T.; Lin, T.L.; Wang, Y.H.; Chen, C.Y. Immunoassay-amplified responses using a functionalized mos2-based spr biosensor to detect Papp-a2 in maternal serum samples to screen for fetal down's syndrome. *Int. J. Nanomed.* **2021**, *16*, 2715–2733. [[CrossRef](#)] [[PubMed](#)]
- Mahmoudpour, M.; Dolatabadi, J.E.N.; Torbati, M.; Homayouni-Rad, A. Nanomaterials based surface plasmon resonance signal enhancement for detection of environmental pollutions. *Biosens. Bioelectron.* **2019**, *127*, 72–84. [[CrossRef](#)]
- Zhang, P.; Chen, Y.P.; Wang, W.; Shen, Y.; Guo, J.S. Surface plasmon resonance for water pollutant detection and water process analysis. *TrAC Trends Anal. Chem.* **2016**, *85*, 153–165. [[CrossRef](#)]
- Song, W.; Guo, X.; Sun, W.; Yin, W.; He, P.; Yang, X.; Zhang, X. Target-triggering multiple-cycle signal amplification strategy for ultrasensitive detection of DNA based on QCM and SPR. *Anal. Biochem.* **2018**, *553*, 57–61. [[CrossRef](#)]
- Li, S.; Xu, J.; Wang, S.; Xia, X.; Chen, L.; Chen, Z. Versatile metal graphitic nanocapsules for SERS bioanalysis. *Chin. Chem. Lett.* **2019**, *30*, 1581–1592. [[CrossRef](#)]
- Shan, Y.; Hu, G.; Grilli, M.L.; He, H.; Zhu, M.; Zhao, Y.; Shao, J. Measuring ultrathin metal coatings using SPR spectroscopic ellipsometry with a prism-dielectric-metal-liquid configuration. *Opt. Express* **2019**, *27*, 7912–7921. [[CrossRef](#)]
- Xue, T.; Qi, K.; Hu, C. Novel SPR sensing platform based on superstructure MoS<sub>2</sub> nanosheets for ultrasensitive detection of mercury ion. *Sens. Actuators B Chem.* **2019**, *284*, 589–594. [[CrossRef](#)]
- Zhang, Z.; Wang, H.; Chen, Z.; Wang, X.; Choo, J.; Chen, L. Plasmonic colorimetric sensors based on etching and growth of noble metal nanoparticles: Strategies and applications. *Biosens. Bioelectron.* **2018**, *114*, 52–65. [[CrossRef](#)] [[PubMed](#)]
- Morisawa, H.; Ono, A.; Inami, W.; Kawata, Y. Hot-electron emission enhancement by deep UV surface plasmon resonance on an aluminum periodic disk-hole array. *Opt. Mater. Express* **2021**, *11*, 2278–2287. [[CrossRef](#)]
- Mishra, A.K.; Mishra, S.K.; Gupta, B.D. SPR based fiber optic sensor for refractive index sensing with enhanced detection accuracy and figure of merit in visible region. *Opt. Commun.* **2015**, *344*, 86–91. [[CrossRef](#)]
- Gong, P.; Li, X.; Zhou, X.; Zhang, Y.; Chen, N.; Wang, S.; Zhao, Y. Optical fiber sensors for glucose concentration measurement: A review. *Opt. Laser Technol.* **2021**, *139*, 106981. [[CrossRef](#)]
- Wang, Y.; Huang, Q.; Zhu, W.; Yang, M.; Lewis, E. Novel optical fiber SPR temperature sensor based on MMF-PCF-MMF structure and gold-PDMS film. *Opt. Express* **2018**, *26*, 1910–1917. [[CrossRef](#)]
- Zhou, J.; Yang, T.; Chen, J.; Wang, C.; Zhang, H.; Shao, Y. Two-dimensional nanomaterial-based plasmonic sensing applications: Advances and challenges. *Coord. Chem. Rev.* **2020**, *410*, 213218. [[CrossRef](#)]
- Karki, B.; Pal, A.; Singh, Y.; Sharma, S. Sensitivity enhancement of surface plasmon resonance sensor using 2D material barium titanate and black phosphorus over the bimetallic layer of Au, Ag, and Cu. *Opt. Commun.* **2022**, *508*, 127616. [[CrossRef](#)]
- Singh, S.; Sharma, A.K.; Lohia, P.; Dwivedi, D.K. Theoretical analysis of sensitivity enhancement of surface plasmon resonance biosensor with zinc oxide and blue phosphorus/MoS<sub>2</sub> heterostructure. *Optik* **2021**, *244*, 167618. [[CrossRef](#)]
- Mostufa, S.; Paul, A.K.; Chakrabarti, K. Detection of hemoglobin in blood and urine glucose level samples using a graphene-coated SPR based biosensor. *OSA Contin.* **2021**, *4*, 2164–2176. [[CrossRef](#)]
- Ouyang, Q.; Zeng, S.; Jiang, L.; Hong, L.; Xu, G.; Dinh, X.Q.; Yong, K.T. Sensitivity enhancement of transition metal dichalcogenides/silicon nanostructure-based surface plasmon resonance biosensor. *Sci. Rep.* **2016**, *6*, 1–13. [[CrossRef](#)]
- Kumar, A.; Yadav, A.K.; Kushwaha, A.S.; Srivastava, S.K. A comparative study among WS<sub>2</sub>, MoS<sub>2</sub> and graphene based surface plasmon resonance (SPR) sensor. *Sens. Actuators Rep.* **2020**, *2*, 100015. [[CrossRef](#)]

22. Dey, B.; Islam, M.S.; Park, J. Numerical design of high-performance WS<sub>2</sub>/metal/WS<sub>2</sub>/graphene heterostructure based surface plasmon resonance refractive index sensor. *Results Phys.* **2021**, *23*, 104021. [[CrossRef](#)]
23. Maharana, P.K.; Jha, R. Chalcogenide prism and graphene multilayer based surface plasmon resonance affinity biosensor for high performance. *Sens. Actuators B Chem.* **2012**, *169*, 161–166. [[CrossRef](#)]
24. Pal, S.; Pal, N.; Prajapati, Y.K.; Saini, J.P. Performance evaluation of SPR biosensor using metamaterial over conventional SPR and graphene based SPR biosensor. In Proceedings of the 2018 5th International Conference on Signal Processing and Integrated Networks (SPIN), Noida, India, 22–23 February 2018; IEEE: Manhattan, NY, USA, 2018; Volume 24, pp. 696–701.
25. Kumar, A.; Kumar, A.; Srivastava, S.K. A study on surface plasmon resonance biosensor for the detection of CEA biomarker using 2D materials graphene, Mxene and MoS<sub>2</sub>. *Optik* **2022**, *258*, 168885. [[CrossRef](#)]
26. Pal, S.; Prajapati, Y.K.; Saini, J.P. Influence of graphene’s chemical potential on SPR biosensor using ZnO for DNA hybridization. *Opt. Rev.* **2020**, *27*, 57–64. [[CrossRef](#)]
27. Pal, S.; Verma, A.; Raikwar, S.; Prajapati, Y.K.; Saini, J.P. Detection of DNA hybridization using graphene-coated black phosphorus surface plasmon resonance sensor. *Appl. Phys. A* **2018**, *124*, 1–11. [[CrossRef](#)]
28. Lin, C.; Chen, S. Design of high-performance Au-Ag-dielectric-graphene based surface plasmon resonance biosensors using genetic algorithm. *J. Appl. Phys.* **2019**, *125*, 113101. [[CrossRef](#)]
29. Prajapati, Y.K.; Srivastava, A. Effect of BlueP/MoS<sub>2</sub> heterostructure and graphene layer on the performance parameter of SPR sensor: Theoretical insight. *Superlattices Microstruct.* **2019**, *129*, 152–162. [[CrossRef](#)]
30. Jia, Y.; Li, Z.; Wang, H.; Cai, H. Sensitivity enhancement of a surface plasmon resonance sensor with platinum diselenide. *Sensors* **2019**, *20*, 131. [[CrossRef](#)]
31. Gan, S.; Zhao, Y.; Dai, X.; Xiang, Y. Sensitivity enhancement of surface plasmon resonance sensors with 2D franckeite nanosheets. *Results Phys.* **2019**, *13*, 102320. [[CrossRef](#)]